Journal of Alloys and Compounds 513 (2012) 460–465

Contents lists available at SciVerse ScienceDirect

Journal of Alloys and Compounds

journal homepage: www.elsevier.com/locate/jallcom

An Fe_3O_4–FeO–Fe@C composite and its application as anode for lithium-ion battery

Xiuyun Zhao [a], Dingguo Xia [b,*], Kun Zheng [c]

[a] College of Environmental and Energy Engineering, Beijing University of Technology, Beijing 100124, China
[b] College of Engineering, Peking University, Beijing 100871, China
[c] Institute of Microstructure and Properties of Advanced Materials, Beijing University of Technology, Beijing 100124, China

ARTICLE INFO

Article history:
Received 5 September 2011
Received in revised form 21 October 2011
Accepted 22 October 2011
Available online 7 November 2011

Keywords:
Iron oxide
Core–shell
Hydrothermal
Anode
Lithium ion battery

ABSTRACT

An Fe_3O_4–FeO–Fe@C composite material has been successfully synthesized by a one-pot hydrothermal method without any templates and a sequential heat treatment process. X-ray diffraction, Raman spectrometry, scanning electron microscopy with energy dispersive spectroscopy, transmission electron microscopy and galvanostatic cell cycling have been used to characterize the structure and electrochemical performance of the as-prepared Fe_3O_4–FeO–Fe@C composite. The electrode shows a stable and reversible capacity of over 600 mAh g^{-1} at a current of 53 mA g^{-1} for up to 60 cycles, which could be ascribed to the unique double-layer core–shell and embedded structures.

1. Introduction

Lithium-ion batteries (LIBs) have been used for various electronic devices because of their unmatched energy density per unit volume or per unit mass. Development of anode materials is crucial for the emerging demands of high power Li-ion batteries. The state-of-the-art anode is graphite with a theoretical capacity of 372 mAh g^{-1} and a potential of 0.1 V relative to Li/Li^+. Recently, much effort has been focused on new anode materials with both larger capacities and slightly more positive insertion voltages with respect to Li/Li^+, in order to minimize any risks of high-surface-area Li plating at the end of a fast recharge [1]. Of these alternatives, iron oxide (Fe_3O_4) has attracted much attention due to its high theoretical specific capacity (926 mAh g^{-1}, one Fe_3O_4 can react with eight lithium ions), safe voltage (~0.9 V vs. Li/Li^+), high electronic conductivity, low cost, natural abundance and non-toxicity [2]. However, like other transition metal oxide anodes, this iron oxide often suffers from poor cycling ability owing to agglomerations and huge volume changes of the active materials during lithium insertion and deinsertion. In order to improve the electrochemical performance of Fe_3O_4, many approaches have been pursued in the literature, such as nanosizing [2–7], carbon-coating and the preparation of a nanosize Fe_3O_4/C composite [8–32].

Nanomaterials play a large role in improving the performance of lithium-ion batteries. Nanoparticles can quickly absorb and store vast numbers of lithium ions without causing deterioration in the electrode since they have large surface areas, short diffusion lengths, and fast diffusion rates [33]. Carbon coating has often been used to improve the cyclability of nanostructured electrode materials in which carbon acts as both a buffering layer for large volume changes and a barrier to prevent aggregation between active particles [34]. Carbon is also introduced into electrodes because of its high electronic conductivity, good lithium permeability, and electrochemical stability [10].

On the other hand, core–shell (carbon) structures have been widely applied in anode materials to improve the electrochemical performance of various metals or metal oxide electrodes [35]. Fe_3O_4@C anode materials have often been synthesized using two-step hydrothermal methods which were either tedious or required environmentally unfriendly or expensive raw materials.

In this work, an iron oxide@carbon (Fe_3O_4–FeO–Fe@C) composite was synthesized by a one-pot hydrothermal method without any templates followed by a sequential heat treatment process in N_2. The electrochemical performance of the Fe_3O_4–FeO–Fe@C composite anode was then investigated. It shows a stable and reversible capacity of over 600 mAh g^{-1} at a current of 53 mA g^{-1} for up to 60 cycles. This could be ascribed to the unique double-layer core–shell structure and embedded structure of the composite.

* Corresponding author. Tel.: +86 10 82529046; fax: +86 10 67396158.
E-mail address: dgxia@pku.edu.cn (D. Xia).

0925-8388/$ – see front matter © 2011 Elsevier B.V. All rights reserved.
doi:10.1016/j.jallcom.2011.10.081

2. Experimental

2.1. Synthesis of Fe_3O_4–FeO–Fe@C composite

All reagents were received from Beijing Chemicals Co. (Beijing, China) and used without further purification. In a typical synthesis process, a mixture of $FeSO_4 \cdot 7H_2O$ (2.34 g) and glucose (0.33 g) with the molar ratio of 5:1 was dissolved in 25 mL deionized water under stirring to form a transparent solution. This solution was transferred and sealed into a 50 mL teflon-lined autoclave, heated at 180 °C for 9 h, and then allowed to cool to room temperature naturally. The precipitate was separated by filtration, washed with deionized water and then vacuum-dried at 80 °C for 12 h to obtain the precursor. The final Fe_3O_4–FeO–Fe@C composite was synthesized by heating the as-prepared precursor at 700 °C for 1 h under a nitrogen atmosphere.

2.2. Structure and compositional characterizations

The crystal structure of the product was characterized by X-ray diffraction (XRD, Bruker D8 Advance, CuKα radiation) and Raman spectroscopy (Renishaw, RM-2000). The morphology was investigated using a field emission scanning electron microscope (SEM, Hitachi S-4300) with an EDAX GENESIS XM2 60S energy dispersive spectroscopy analyzer and transmission electron microscopes (TEM, JEM-2010 and JEM-2010F). Thermogravimetric analysis (TGA) was carried out on a TG/DTA6300 thermal analyzer with a heating rate of 5 °C min^{-1} in a flowing air atmosphere.

2.3. Electrochemical characterizaition

The electrochemical performance was evaluated using CR2032 coin cells with a NEWARE BTS. The test electrode was prepared by casting a slurry consisting of the as-prepared powder, acetylene black and polytetrafluoroethylene (PTFE) in a weight ratio of 80:10:10 on a stainless steel foil, followed by drying at 80 °C for 12 h under a vacuum. Coin-type cells were assembled in an argon-filled dry glove box with lithium foil as the counter and reference electrodes, 1 M $LiPF_6$ in EC/DMC (1:1 vol%) as an electrolyte, and a Whatman GF/D borosilicate glass-fibre sheet as a separator. The cells were discharge-charged at various values of constant current in the voltage range of 0.005–3.0 V (vs. Li/Li^+). Cyclic voltammetry (CV) measurement was conducted at 0.05 mV s^{-1} within the range of 3.0–0.0 V on a VMP3 (Princeton Applied Research).

3. Results and discussion

3.1. Microstructure characterization

To clarify the crystal structure of as-prepared Fe_3O_4–FeO–Fe@C composite, XRD experiments were carried out. Fig. 1(a) shows the XRD patterns of the final composite, which is in agreement with Fe_3O_4, FeO and Fe (JCPDS card No. 01-089-0691, No. 01-077-2355, No. 01-087-0721, respectively). No obvious peaks corresponding to crystalline carbon can be observed. However, amorphous carbon created from glucose cannot be excluded. The Raman spectroscopic analysis indicates a D-band at 1332 cm^{-1} and a G-band at 1601 cm^{-1}, with similar intensities (Fig. 1(b)), which confirms the amorphous carbon structure [11]. Thermal gravimetric analysis (TGA) was used to assess the carbon content of the sample. In Fig. 2, we note a slight weight uptake starting near 200 °C in air, corresponding to when Fe_3O_4, FeO and Fe in the composite are transformed into α-Fe_2O_3, followed by a 43.2% weight loss occurring near 400 °C extending to 600 °C, indicating oxidation of carbon in the sample.

To further investigate the structure of the Fe_3O_4–FeO–Fe@C composite, energy-dispersive X-ray (EDX) spectra and elemental mapping characterizations were carried out. Fig. 3(a) shows the EDX spectrum of the composite corresponding to the region marked with a red box (Fig. 3(b)). The peaks corresponding to C, O and Fe are clearly identified. From the elemental maps (Fig. 3(c)–(e)) we found that the iron oxide (or Fe) and carbon are blended together. The detailed crystal structure and substructure of the Fe_3O_4–FeO–Fe@C composite was further analyzed by TEM and high-resolution transmission electron microscopy (HRTEM) analysis. Representative SEM and TEM images of the as-prepared Fe_3O_4–FeO–Fe@C composite are shown in Fig. 4(a)–(d). It can be seen from Fig. 4(a) and (b) that roughly spherical particles are dispersed and embedded in the carbon matrix uniformly. Observed

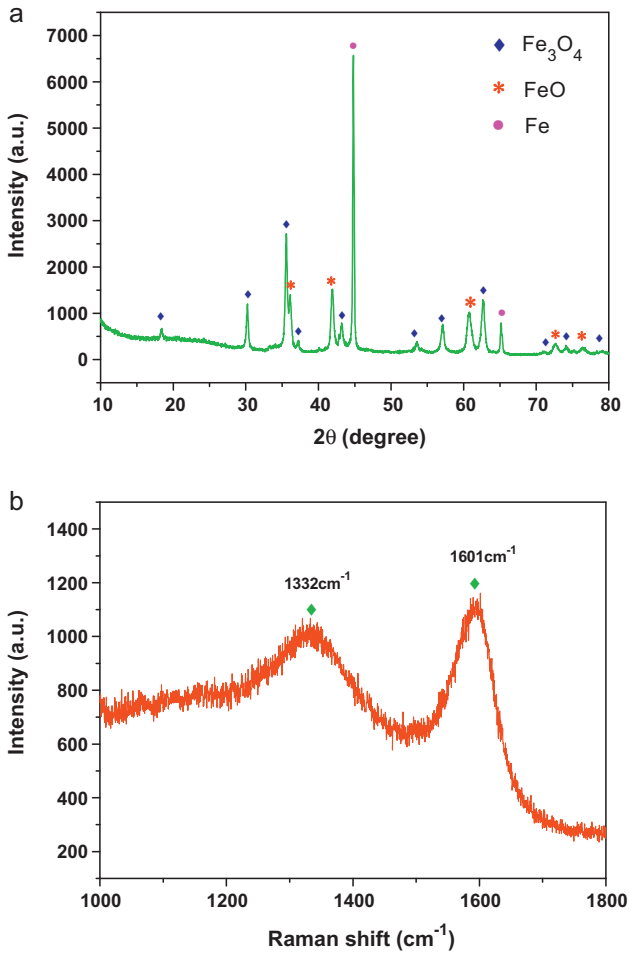

Fig. 1. (a) XRD pattern and (b) Raman spectrum of as-prepared Fe_3O_4–FeO–Fe@C composite.

in Fig. 4(c), the diameters of these core–shell particles embedded in the matrix are about 20–30 nm. Fig. 4(d) shows the high-resolution transmission electron microscopy (HRTEM) image of a single nanoparticle in which both the outer carbon layer and the inner core can be clearly observed. The amorphous carbon layer, which has a thickness of ~4–7 nm, is uniform and continuous. Inter-

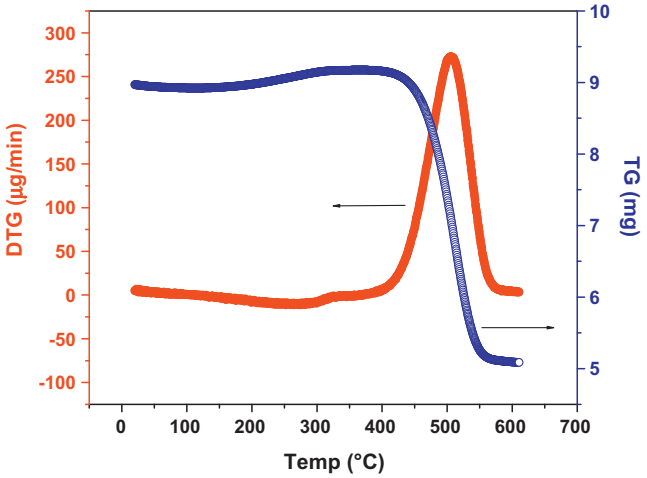

Fig. 2. TG-DTG curves of as-prepared Fe_3O_4–FeO–Fe@C composite in air.

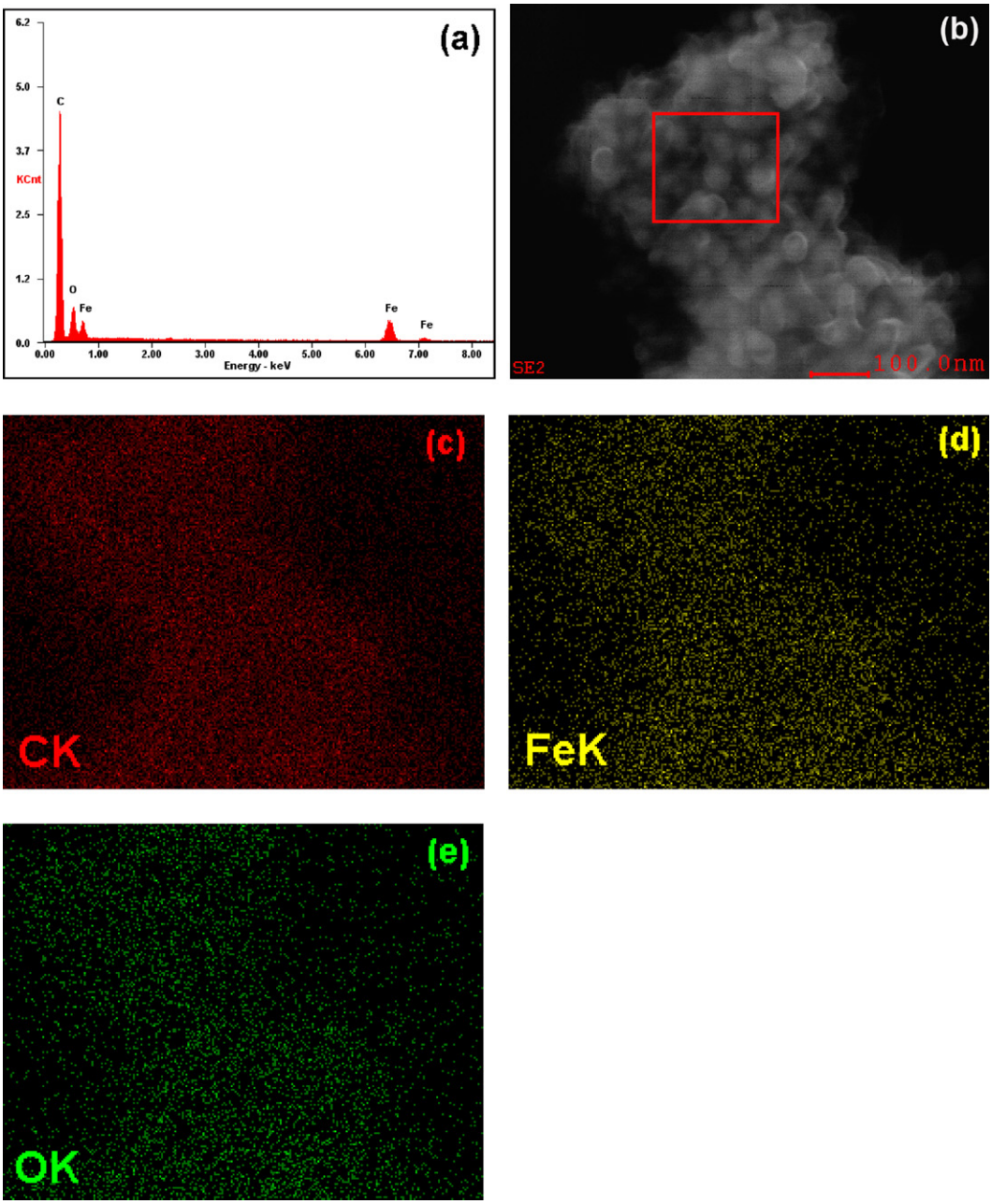

Fig. 3. (a) EDX spectrum; (b) SEM image; and (c) elemental maps of C, Fe and O in Fe_3O_4–FeO–Fe@C composite.

estingly, we found a double-layer core wrapped by the carbon shell. The core region immediately next to the carbon shell displays lattice fringes with an inter-planar spacing of 0.202 nm, which is good agreement with that of the (1 1 0) plane of Fe corresponding to $2\theta = 44.7^\circ$. The inner core gives a spacing of 0.252 nm, indexed to the (3 1 1) plane of Fe_3O_4. The lattice fringes of FeO have not been resolved in this HRTEM image, possibly due to smallness of the region or the metastable state of FeO. FeO is deduced to lie between the Fe layer and Fe_3O_4, because the nearer it is to the carbon layer, the more likely will the region be reduced.

3.2. Electrochemical performance

In order to test the applicability of this Fe_3O_4–FeO–Fe@C composite as an anode in lithium-ion batteries, the electrochemical properties of Li insertion/extraction were investigated. Fig. 5(a) presents typical discharge/charge curves of the Fe_3O_4–FeO–Fe@C composite anode for the 1st, 2nd, 10th, 30th and 60th cycle, at a rate of 88 mA g^{-1}. The first discharge capacity is 1722 mAh g^{-1} and a high and stable discharge capacity of over 550 mAh g^{-1} was obtained after 60 cycles. Clearly, the 60th and 30th discharge curves overlap, which indicates that this core–shell electrode has good cycling stability. The discharge plateau potential is around 0.8 V in the first cycle and then changes during the subsequent cycles. It increases first to about 1.0 V in the 2nd cycle, and then decreases to about 0.75 V, remaining at this level for the following discharge process. This discharge platform can enhance the security of batteries compared with that of graphite anode. The voltage hysteresis of this composite electrode can also be observed in the lithiation/delithiation process, which may be ascribed to the existence of a large amount of amorphous carbon and conversion mechanism itself [36].

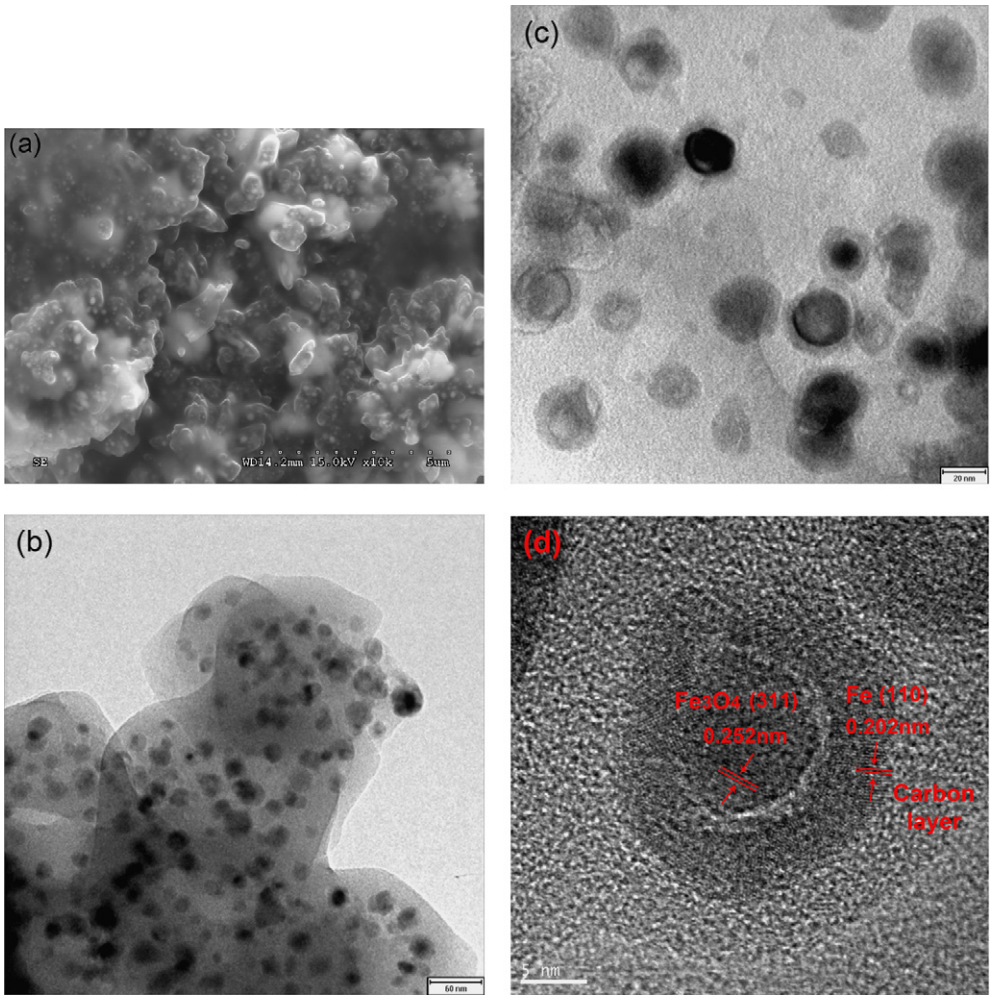

Fig. 4. (a) SEM, (b) TEM, (c) high magnification TEM, and (d) HRTEM images of as-prepared Fe_3O_4–FeO–Fe@C composite.

The specific discharge/charge capacities at various current rates were measured to evaluate the cycle performances of the Fe_3O_4–FeO–Fe@C electrode. Fig. 5(b) plots the relative specific capacities of batteries versus cycle numbers. Stable reversible capacities of 600 mAh g^{-1} and 550 mAh g^{-1} are obtained at cycling rates of 53 mA g^{-1} and 88 mA g^{-1}. Increasing the rate to 176 mA g^{-1}, this core–shell electrode can still deliver a reversible capacity of over 400 mAh g^{-1} in the first 40 cycles. When continuously increasing the rate to 352 mA g^{-1}, the capacity of the electrode fades gradually. This capacity fading may result from the degradation of the electrical contacts between active particles and the loose carbon layers under strong current shock. In this work the mass of Fe is included when calculating the specific capacity of Fe_3O_4–FeO–Fe@C composite, although the metallic iron is traditionally considered to be inactive for lithium storage. Metallic iron is considered to improve the electronic connection from active materials to a current collector [4]. In addition, the contribution of the carbon in the electrochemical process is estimated to about 24% by the calculation method described in Ref. [34].

To further understand the electrochemical process, cyclic voltammetry (CV) curves of this nanocomposite were recorded for the first four cycles in the voltage range between 3.0 V and 0.0 V at a scan rate of 0.05 mV s^{-1}, as shown in Fig. 5(c). In the first cycle, there are two peaks observed in the cathodic process. A broad peak appears at 0.57 V, which can be associated with the reduction of Fe^{3+} and Fe^{2+} to Fe^0 [19]:

$$(1)Fe_3O_4 + 8Li \rightarrow 3Fe^0 + 4Li_2O$$

$$(2)FeO + 2Li \rightarrow Fe^0 + Li_2O$$

In addition, there is another tiny peak at 1.3 V, which is ascribed to the irreversible reaction related to the decomposition of the electrolyte. Two anodic peaks are present at 1.6 V and 1.86 V, corresponding to the oxidation of Fe^0–Fe^{3+} [16]:

$$3Fe^0 + 4Li_2O \rightarrow Fe_3O_4 + 8Li \quad (3)$$

During the anodic process, both the peak current and the integrated area of the anodic peak are reduced, indicating capacity loss during the charging process. This is consistent with the results of the discharge/charge test. In subsequent cycles, the cathodic and anodic peak potentials shift positively compared with the first cycle. The CV curves of the Fe_3O_4–FeO–Fe@C composite electrode are stable and show good reversibility after the first cycle.

The enhanced electrochemical performance of the Fe_3O_4–FeO–Fe@C composite anode is due to the presence of the carbon shell and carbon matrix around core–shell nanoparticles. Firstly, the amorphous carbon (especially in the form of a carbon shell) can improve the electrical conductivity of the electrode because continuous carbon coatings can form a more efficient electron conductive network. Secondly, the carbon

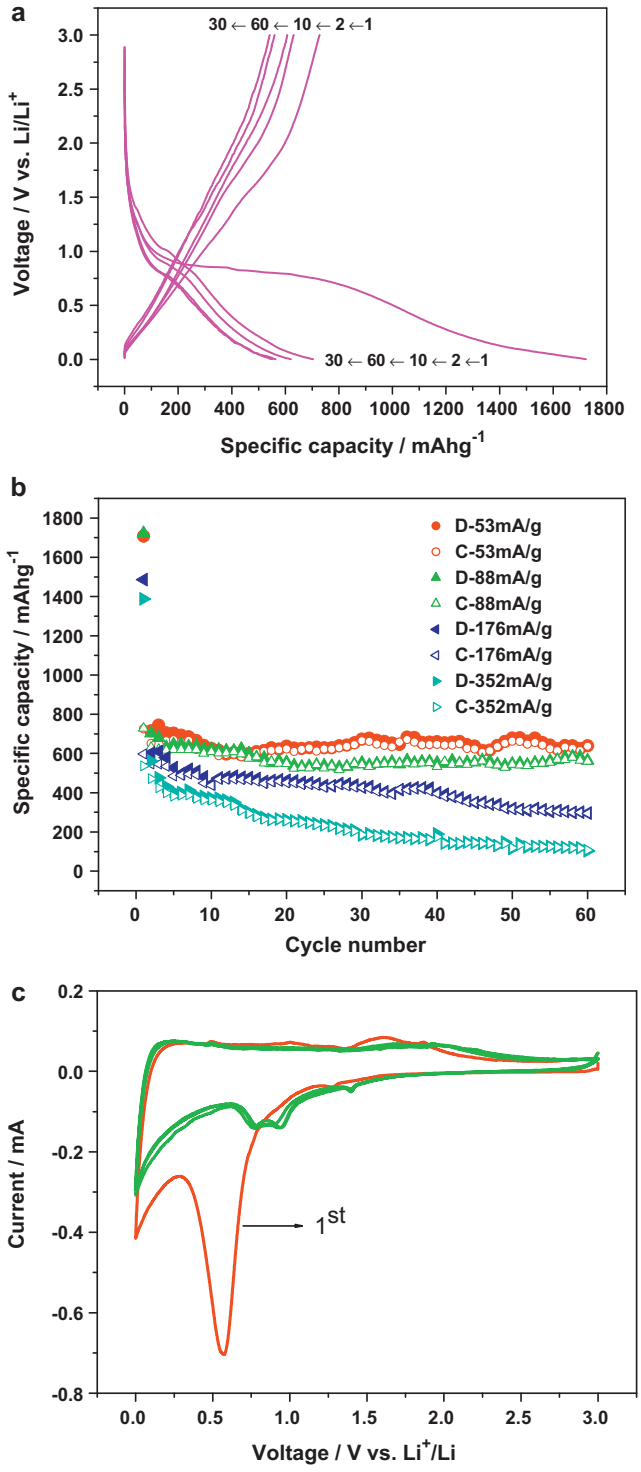

Fig. 5. (a) Voltage profiles at 88 mA g^{-1} and (b) cycling performance at various current rates of Fe_3O_4–FeO–Fe@C composite. D and C refer to discharge and charge, respectively.

shell and carbon matrix act as barriers to prevent any aggregation between active nanoparticles. Thirdly, carbon functions as a buffering layer for the large volume changes in the discharge/charge process (cushion effect). Note that the high irreversible capacity loss found only in the first cycle is ascribed to electrolyte reduction and the formation of solid electrolyte interphase (SEI) films on the electrode surface, which consume much of the Li. It is possibly because this core–shell composite contains much amorphous carbon, which has a high surface area. Therefore, low initial coulombic efficiency and large voltage hysteresis of this composite electrode needs further improvement.

4. Conclusions

In summary, we have successfully synthesized an Fe_3O_4–FeO–Fe@C composite anode material by a one-pot hydrothermal method without any templates followed by a sequential heat treatment process. The electrode shows a stable and reversible capacity of over 600 mAh g^{-1} at a current of 53 mA g^{-1} between 0 V and 3.0 V for up to 60 cycles. This can be ascribed to the unique double-layer core–shell structure and embedded structure which improve electrical conductivity of the electrode, prevent the aggregation of active nanoparticles and provide a buffer for the large volume changes in the discharge/charge process. The experimental results suggest that the Fe_3O_4–FeO–Fe@C composite has a potential application as anode material for Li-ion batteries.

Acknowledgement

This work was supported by the major program of Beijing Municipal Natural Science Foundation (No. 20110001).

References

[1] J.M. Tarascon, M. Armand, Nature 414 (2001) 359–367.
[2] L. Taberna, S. Mitra, P. Poizot, P. Simon, J.M. Tarascon, Nat. Mater. 5 (2006) 567–573.
[3] H.N. Duan, J. Gnanaraj, X.P. Chen, B.Q. Li, J.Y. Liang, J. Power Sources 185 (2008) 512–518.
[4] G.H. Lee, J.G. Park, Y.M. Sung, K.Y. Chung, W. Il Cho, D.W. Kim, Nanotechnology 20 (2009) 295205.
[5] S.Q. Wang, J.Y. Zhang, C.H. Chen, J. Power Sources 195 (2010) 5379–5381.
[6] S. Mitra, P. Poizot, A. Finke, J.M. Tarascon, Adv. Funct. Mater. 16 (2006) 2281–2287.
[7] S.B. Ni, D.Y. He, X.L. Yang, T. Li, J. Alloys Compd. 509 (2011) L305–L307.
[8] W.M. Zhang, X.L. Wu, J.S. Hu, Y.G. Guo, L.J. Wan, Adv. Funct. Mater. 18 (2008) 3941–3946.
[9] L. Wang, Y. Yu, P.C. Chen, D.W. Zhang, C.H. Chen, J. Power Sources 183 (2008) 717–723.
[10] T. Muraliganth, A.V. Murugan, A. Manthiram, Chem. Commun. 47 (2009) 7360–7362.
[11] Y.Z. Piao, H.S. Kim, Y.E. Sung, T. Hyeon, Chem. Commun. 46 (2010) 118–120.
[12] Z.M. Cui, L.Y. Hang, W.G. Song, Y.G. Guo, Chem. Mater. 21 (2009) 1162–1166.
[13] H. Liu, G.X. Wang, J.Z. Wang, D. Wexler, Electrochem. Commun. 10 (2008) 1879–1882.
[14] M. Zhang, D.N. Lei, X.M. Yin, L.B. Chen, Q.H. Li, Y.G. Wang, T.H. Wang, J. Mater. Chem. 20 (2010) 5538–5543.
[15] C.M. Ban, Z.C. Wu, D.T. Gillaspie, L. Chen, Y.F. Yan, J.L. Blackburn, A.C. Dillon, Adv. Mater. 22 (2010) E145–E149.
[16] Y. He, L. Huang, J.S. Cai, X.M. Zheng, S.G. Sun, Electrochim. Acta 55 (2010) 1140–1144.
[17] S.L. Jin, H.G. Deng, D.H. Long, X.J. Liu, L.A. Zhan, X.Y. Liang, W.M. Qiao, L.C. Ling, J. Power Sources 196 (2011) 3887–3893.
[18] G.M. Zhou, D.W. Wang, F. Li, L.L. Zhang, N. Li, Z.S. Wu, L. Wen, G.Q. Lu, H.M. Cheng, Chem. Mater. 22 (2010) 5306–5313.
[19] J.Z. Wang, C. Zhong, D. Wexler, N.H. Idris, Z.X. Wang, L.Q. Chen, H.K. Liu, Chem. Eur. J. 17 (2011) 661–667.
[20] P.C. Lian, X.F. Zhu, H.F. Xiang, Z. Li, W.S. Yang, H.H. Wang, Electrochim. Acta 56 (2010) 834–840.
[21] B.J. Li, H.Q. Cao, J. Shao, M.Z. Qu, J.H. Warner, J. Mater. Chem. 21 (2011) 5069–5075.
[22] W.H. Shi, J.X. Zhu, D.H. Sim, Y.Y. Tay, Z.Y. Lu, X.J. Zhang, Y. Sharma, M. Srinivasan, H. Zhang, H.H. Hng, Q.Y. Yan, J. Mater. Chem. 21 (2011) 3422–3427.
[23] P. Wu, N. Du, H. Zhang, J.X. Yu, D.R. Yang, J. Phys. Chem. C 115 (2011) 3612–3620.
[24] S.M. Yuan, J.X. Li, L.T. Yang, L.W. Su, L. Liu, Z. Zhou, Acs Appl. Mater. Interfaces 3 (2011) 705–709.
[25] E. Kang, Y.S. Jung, A.S. Cavanagh, G.H. Kim, S.M. George, A.C. Dillon, J.K. Kim, J. Lee, Adv. Funct. Mater. 21 (2011) 2430–2438.
[26] S.M. Yuan, Z. Zhou, G. Li, CrystEngComm 13 (2011) 4709–4713.
[27] Z.C. Yang, J.G. Shen, L.A. Archer, J. Mater. Chem. 21 (2011) 11092–11097.
[28] J. Su, M.H. Cao, L. Ren, C.W. Hu, J. Phys. Chem. C 115 (2011) 14469–14477.
[29] T. Zhu, J.S. Chen, X.W. Lou, J. Phys. Chem. C 115 (2011) 9814–9820.

[30] H. Duan, J. Gnanaraj, J.Y. Liang, J. Power Sources 196 (2011) 4779–4784.
[31] G. Wang, T. Liu, X.L. Xie, Z.Y. Ren, J.B. Bai, H. Wang, Mater. Chem. Phys. 128 (2011) 336–340.
[32] L.W. Ji, Z.K. Tan, T.R. Kuykendall, S. Aloni, S.D. Xun, E. Lin, V. Battaglia, Y.G. Zhang, Phys. Chem. Chem. Phys. 13 (2011) 7139–7146.
[33] Y.G. Guo, J.S. Hu, L.J. Wan, Adv. Mater. 20 (2008) 2878–2887.
[34] K.T. Lee, Y.S. Jung, S.M. Oh, J. Am. Chem. Soc. 125 (2003) 5652–5653.
[35] X.W. Lou, L.A. Archer, Z.C. Yang, Adv. Mater. 20 (2008) 3987–4019.
[36] M.R. Palacin, J. Cabana, L. Monconduit, D. Larcher, Adv. Mater. 22 (2010) E170–E192.